Materials Advances

ROYAL SOCIETY OF CHEMISTRY

COMMUNICATION

View Article Online
View Journal | View Issue

Cite this: *Mater. Adv.*, 2020, 1, 584

Received 25th April 2020,
Accepted 17th June 2020

DOI: 10.1039/d0ma00243g

rsc.li/materials-advances

Metal-free coumarate based ionic liquids and poly(ionic liquid)s as corrosion inhibitors†

Esther Udabe,*[a] Maria Forsyth,[abc] Anthony Somers[b] and David Mecerreyes[ac]

Mild steel is used extensively in infrastructure and its corrosion susceptibility is a severe issue both economically and with regards to safety. The toxicity of traditional chromate inhibitors requires the discovery of new non-toxic anti-corrosion solutions. Here we show metal-free organic ionic liquids that can be used as direct anodic and cathodic corrosion inhibitors or incorporated into a polymer coating. New *p*-coumarate methacrylic UV curable ionic liquids that can be used as direct corrosion inhibitors or incorporated into a polymer coating are reported.

Mild steel, having no more than 2% carbon and no other appreciable alloying element, makes up the largest part of steel production and is used in a vast range of applications, from concrete reinforcement and small machine parts to containers and construction materials.[1,2] However, despite its relatively low cost and good mechanical properties, mild steel is prone to undergo severe corrosion[1] leading to high economic and safety losses. For this reason, understanding and mitigating corrosion of such alloys is of primary importance. Among the different corrosion protection methods, the use of chemical inhibitors and coatings are the most commonly used.[3] Corrosion inhibitors can be incorporated as an additive into a paint coating to protect external structures or added to water tanks and pipeline streams to protect the mild steel internal surfaces.[3] Generally, most chemical inhibitors reduce the rate of corrosion by forming a passive adsorption layer on the metal surface.[3–5] Chromate based inhibitors loaded into different coatings are known to be the most efficient anticorrosive method for a large range of metals and alloys, reducing both the anodic and cathodic reactions that result in corrosion and metal loss.[6] However, hexavalent chromium was banned due its high toxicity, and thus, alternative and non-toxic chemical inhibitors are needed in order to replace these highly efficient chromate-based compounds.[6] One very promising family of chromium-free chemical inhibitors recently demonstrated has been the rare earth carboxylate compounds. These compounds can suppress both the anodic and cathodic reactions that are involved in corrosion, showing a synergistic effect between the rare earth metal and the carboxylates.[6–8] Among these, rare earth metal aromatic carboxylates have demonstrated the best anticorrosive performance due to the formation of a passive barrier layer that forms due to adsorption and subsequent reaction with the underlying alloy substrate.[7,9,10] From this past work, it is evident that the aromatic carboxylate, *p*-coumarate, provides very efficient inhibition.[2,11–14] For instance, when comparing lanthanum 3-(4′-hydroxyphenyl)propionate with lanthanum (*p*-coumarate)$_3$, Deacon *et al.* demonstrated that the coumarate with the unsaturated double bond in the side group provides better surface passivation than the aliphatic propionate group.[12] In fact, it is reported that the carboxylate group has the ability to create a hydrogen bond with the hydroxide groups of the surface, that contributes to the formation of surface complexes which acts as a barrier against corrosion.[15,16]

Interestingly, metal-free organic inhibitors such as ionic liquids have also shown promising performance in corrosion applications and are of great interest due to their effectiveness at wide range of temperatures, compatibility with protected materials, good solubility in water, low costs and relatively low toxicity.[17] In a pioneering work, Alison L. Chong *et al.* reported synthesis of salts based on imidazolium cation and carboxylate anions showing an effective corrosion inhibition.[18] More precisely, they found that 2-methylimidazolinium *p*-coumarate was a most effective inhibitor, showing a strong anodic inhibition effect.[18] Aside from the aforementioned salts, inhibitor compounds that can be incorporated into a polymer coating have great potential, since they can add their intrinsic inhibition effect to the protective layer effect of a polymer coating.

In this work, we present a series of easy to make methacrylic monomeric organic salts. First, we investigate their use and

[a] *POLYMAT University of the Basque Country UPV/EHU, Joxe Mari Korta Center, Donostia-San Sebastian 20018, Spain*
[b] *Institute for Frontier Materials, Deakin University, Geelong, Victoria, 3220, Australia*
[c] *IKERBASQUE Basque Foundation for Science, Bilbao, Spain*

† Electronic supplementary information (ESI) available. See DOI: 10.1039/d0ma00243g

properties as corrosion inhibitors and then we show a proof of concept of their easy integration into an anticorrosion polymer coating.

For this purpose three different coumarate based ionic monomers (a–c) were synthesized as described in the ESI.† First, the ionic monomer a [*p*-OHcoum] MA was easily obtained by instantaneous acid–base proton exchange reaction between commercially available 2-dimethylaminoethyl methacrylate and *p*-coumaric acid (Scheme S1B, ESI†). Moreover, it is known that inhibition efficiency increases with an increase in the anion or cation size or aliphatic chain length.[18,19] For this reason, two additional monomers were synthesized using as reactants 2-dimethylaminoethyl methacrylate and butoxy *p*-coumaric acid and hexoxy *p*-coumaric acid leading to two additional monomers [*p*-O(C_4H_9)coum] MA and [*p*-O(C_6H_{13})coum] MA, b and c respectively.

First, the corrosion inhibition properties of the monomers were evaluated by immersing mild steel AS1020 foils into an aqueous solution of the ionic monomers. By this method it is expected that the anionic coumarate may self-assemble and adsorb onto the mild steel surface. Potentiodynamic polarisation scans of AS1020 mild steel after an exposure of 24 h in control (0.01 M NaCl) and solutions of inhibitors (0.01 M NaCl + 8 mM inhibitor monomers) are shown in Fig. 1B. Corrosion potentials (E_{corr}), corrosion current density (i_{corr}), anodic and cathodic Tafel slopes (β_a and β_c) calculated using Tafel extrapolation are reported in Table S1 in the ESI.† After 24 h of immersion in 0.01 M NaCl aqueous solution, [*p*-OHcoum] MA, [*p*-O(C_4H_9)-coum] MA and [*p*-O(C_6H_{13})coum] MA monomers suppressed the anodic activity as compared to the control without ionic liquid monomer. The corrosion potential (E_{corr}) of [*p*-OHcoum] MA shifted towards a more positive potential from −0.523 V to −0.012 V, showing a corrosion current density (i_{corr}) of 0.009 μA and an inhibitor efficiency of 99.0%. [*p*-O(C_4H_9)coum] MA shifted the E_{corr} towards a positive potentials, from −0.523 V to −0.140 V, representing a corrosion current density (i_{corr}) of 0.026 μA and an inhibitor efficiency of 97.2%. Finally, the compound with the hexyl substituent on the coumarate, [*p*-O(C_6H_{13})coum] MA, shifted the E_{corr} towards a positive potentials, from −0.523 mV to −0.147 V, representing a corrosion current density (i_{corr}) of 0.008 μA and an inhibitor efficiency of 99.1%. Moreover, the variation of Tafel slopes of the monomer solution (shown in Table S1 of ESI†) comparing with the control means that the inhibitors influence the anodic and the cathodic corrosion reaction on mild steel.[19] To sum up, the PP curves suggest that these coumarate based monomers mainly affect and suppress the anodic activity. The extensive noise observed in particular with the with the [*p*-OHcoum] MA monomer is

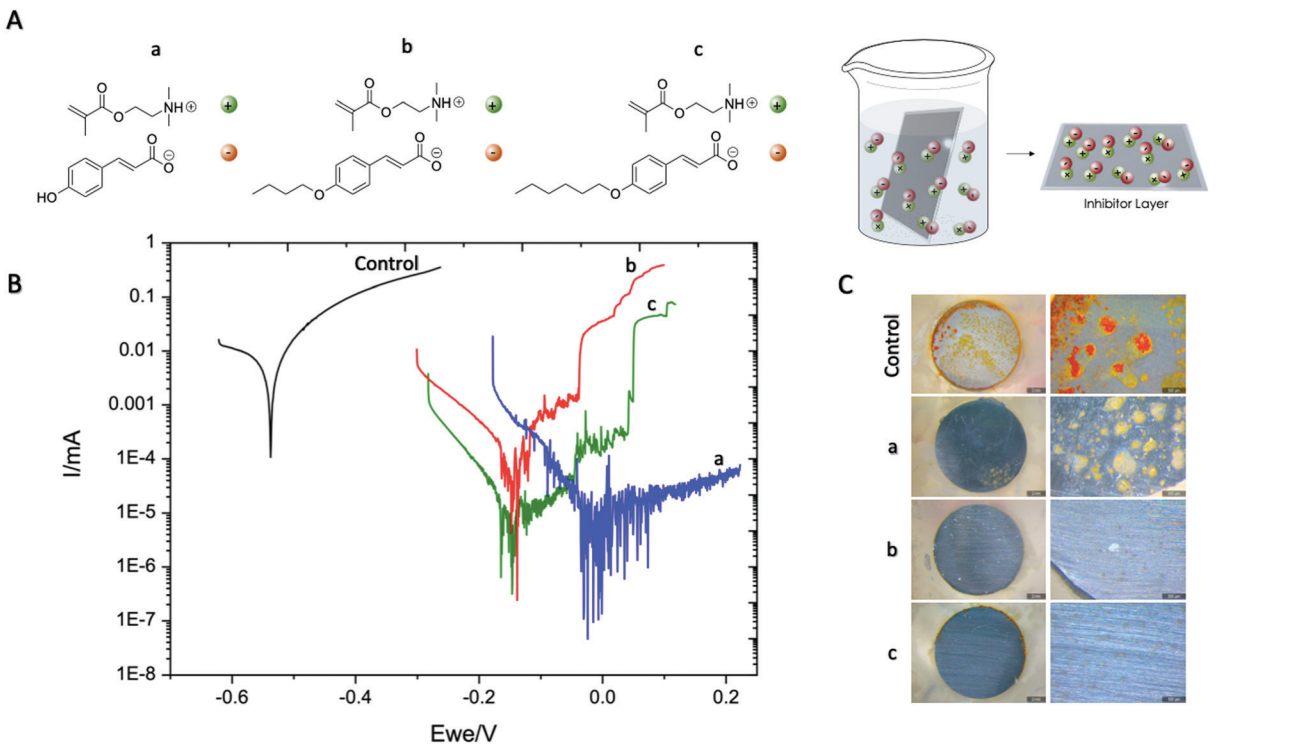

Fig. 1 Chemical structures. (A) Chemical structures of monomers, (a) 2-(dimethylamino)ethyl methacrylate *p*-coumarate ([*p*-OHcoum] MA), (b) 2-(dimethylamino)ethyl methacrylate butoxy *p*-coumarate ([*p*O(C4H9)coum] MA) and (c) 2-(dimethylamino)ethyl methacrylate hexoxy *p*-coumarate and ([*p*O(C6H13)coum] MA). Representation of an immersion of mild steel 1020 surface in an aqueous solution containing ionic liquid monomer inhibitors (B). Potentiodynamic polarisation results of AS1020 mild steel after 24 h at OCV in control (black) and inhibited solutions containing 8 mM of [*p*-OHcoum] MA (a: red), [*p*-O(C_4H_9)coum] MA (b: blue) and [*p*-O(C_6H_{13})coum] MA (c: green) (B) and optical microscopy images (C) of mild steel samples immersed in the control (water only) and the aqueous solutions containing ionic liquid monomers (a: [*p*OHcoum] MA, b: [*p*-O(C_4H_9)coum] MA) and c: ([*p*-O(C_6H_{13})coum] MA) for 24 h.

suggesting that there is ongoing activity on the steel surface; for example, metastable pitting with the inhibitor suppressing pit growth which is also observed from the optical microscopy in Fig. 1C(a) where deposits are spotted across the steel substrate. It appears that [*p*-O(C_6H_{13})coum] MA providing the best inhibition in solution and a significant increase in the pitting potential, which again is evident in the optical microscopy image in Fig. 1C(c) with an almost pristine surface. SEM images of these surfaces immersed for 24 hours show a similar trend (Fig. S3, ESI†).

Electrochemical impedance spectroscopy (EIS) measurements of different solutions to further understand the corrosion inhibition effect of the ionic monomers. Fig. 2 and Fig. S2 (ESI†) represent the impedance response of each monomer comparing to the control surface without monomer. The Bode plots shows the impedance response of stainless steel surfaces covered by [*p*-OHcoum] MA, [*p*-O(C_4H_9)coum] MA and [*p*-O(C_6H_{13})coum] MA monomers during an immersion on 0.01 M NaCl aqueous solution for 24 h. The control surface (Fig. 2a and c) shows a decrease in the impedance and in the plateau of the phase angle in the low frequency range (10^{-1}–10^{1} Hz) with time. Mild steel, after an immersion of 2 h in [*p*-OHcoum] MA solution, presents an impedance of $10^{4.25}$ Ω, this value increases until $10^{5.5}$ Ω after 24 hours.

These increasing low frequency responses with time indicates that the inhibitor adsorbs and creates a barrier over the whole surface forming a protective layer against corrosive NaCl environment.[20] In the case of the mild steel immersed in an aqueous solution containing the [*p*-O(C_4H_9)coum] MA monomer, the impedance value is 10^5 Ω in the low frequency range with a corresponding phase angle of 72°. The Bode plots for the [*p*-O(C_6H_{13})coum] MA monomer presents an impedance of $10^{5.7}$ Ω at the low frequency range, which is better than either [*p*-OHcoum] MA or [*p*-O(C_4H_9)coum] MA monomers. In the corresponding phase angle a plateau is observed at 78° is obtained, indicating that [*p*-O(C_6H_{13})coum] MA inhibitor presents the highest capacitive behaviour consistent with the best anticorrosive performance also observed from immersion and PP studies. This data suggests that the presence of all monomers decreased the corrosion rate of mild steel AS1020 through the development of a passive film on the alloy surface. As a first conclusion, [*p*-O(C_6H_{13})coum] MA having an hexyl chain presented the best corrosion inhibition effect among the three monomers.[21,22]

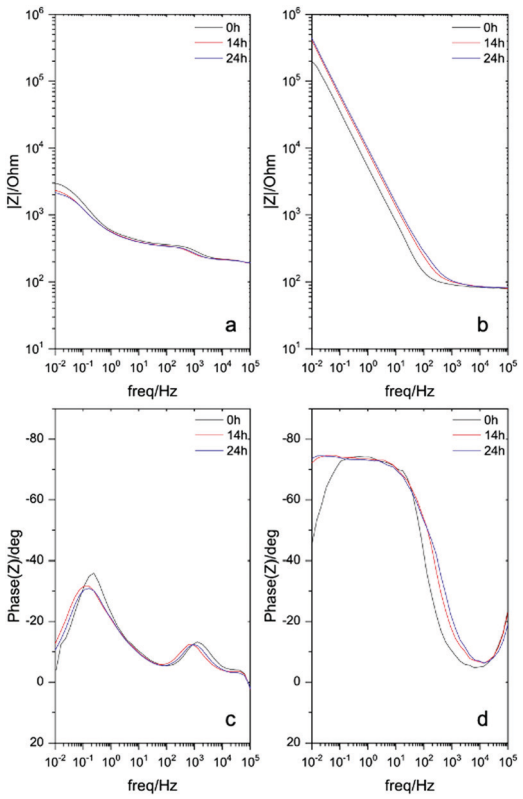

Fig. 2 Electrochemical impedance spectra for AS1020 mild steel immersed in the control and the inhibited solutions up to 24 h: impedance modulus and phase angle plots for control (a and c); inhibited solution containing [*p*-O(C_6H_{13})coum] MA (b and d).

To further understand this corrosion inhibition behaviour, imaging of the surfaces using both optical and SEM techniques were undertaken. Fig. 1C presents optical images of the samples immersed in control, [*p*-OHcoum] MA and [*p*-O(C_6H_{13})coum] MA. The control samples are covered with red rust, while the inhibitor immersed surfaces present minor corrosive attack and a thin and adherent surface protective film, showing some inhibitor-based crystals attached to the surface. On the other hand, Fig. S3–S7 (ESI†) present surface analysis of the samples immersed in solutions with and without inhibitors characterized by SEM and EDS. In each sample, two main areas were selected for the EDS analysis: inhibitor crystals covered and uncovered areas. For the control sample surface analysis, the main deposits consist on a mixture of iron oxide, being the corrosion product precipitated on the surface. On the other hand, samples in contact with both inhibitor monomers ([*p*-OHcoum] MA, [*p*-O(C_4H_9)coum] MA and [*p*-O(C_6H_{13})coum] MA) exhibit less corrosion products (as shown in the optical images, Fig. 1C) and the crystals that are precipitated on the surface contain nitrogen, an atom that is present in the monomers. Therefore, it can be concluded that the inhibitor may deposit and create crystals on the surface in order to stop steel dissolution in form of corrosion pitting.

With respect to the corrosion inhibition mechanism, it can be said that the inhibition efficiency of inhibitors in mild steel is mainly determined by the length of the hydrophobic tails attached to coumarate anion the electrostatic interaction of the head groups with the metal substrate. It is reported that increasing the alkyl chain length facilitates the formation of a compact film at the steel/solution inter-face, resulting in a pronounced surface coverage and improved inhibition of corrosion.[23] Earlier work by Seter *et al.* proposed a similar effect with the position of the OH of different derivatives of coumaric acid affecting packing on the surface and inhibition.[24] Yousefi *et al.* demonstrated that the steel surface is covered with the aromatic ring and the alkyl chains present in the inhibitors. In our case, the positive charge on the nitrogen atom is delocalized, resulting in a low net positive charge on the whole structure. The charge delocalization of the nitrogen may show less repulsive force with the positive charge present on

the steel surface,[21] allowing a better interaction between inhibitors and mild steel. Moreover, the π-electrons of the aromatic rings and the oxygen atom present in the coumarate anion accompanying a good distribution of the negative charge, can interact with the metal vacant d-orbital to prevent metal dissolution in order to generate a protective passive layer against corrosion (Fig. 1A).

Next the ionic liquid monomers were introduced into polymeric coatings by UV-photopolymerization. A typical UV-photopolymerization formulation (see ESI† and Scheme 1) was chosen as a reference to which a given amount of ionic monomer was introduced (20 wt%). The monomer liquid mixture was deposited onto mild steel and UV photopolymerize, forming a crosslinked polymer coating on top of the steel substrate, as shown in Fig. 3. The UV photopolymerization was observed optically with the appearance of a transparent coating and the acrylic bond dissapearance was confirmed by FTIR (Fig. S10–S12, ESI†). As a result, a cross-linked polymer network is obtained in which the ammonium cation is covalently attached whereas the coumarate free anions are interacting ionically. EIS measurements of different coated mild steels (coating thickness 60 micrometers) samples were carried out in order to represent an impedance response of each coating containing the ionic monomer inhibitors in comparison to the control polymer coating without ionic monomer. Fig. 3A showed polymer coatings on AS1020 mild steel containing 20% of [*p*-OHcoum] MA, 20% of [*p*-O(C_4H_9)coum] MA, and 20% of [*p*-O(C_6H_{13})coum] MA after an immersion of 20 h in 0.005 M NaCl. It was observed that [*p*-OHcoum] MA take water during immersion. During the water swelling test (see ESI,† Experimental part) it was observed also that [*p*-OHcoum] MA increased its mass in 32% after 72 h (Fig. S13, ESI†). On the other hand, increasing the length of the alkyl chain attached to the oxygen of the coumarate anion, the hydrophobicity is increased and so the weight of [*p*-O(C4H9)coum] MA and [*p*-O(C6H13)coum] MA remained constant. It is concluded that for coatings containing 20% [*p*-O(C_4H_9)coum] MA and 20% [*p*-O(C_6H_{13})coum] MA, water swelling does not happen, due to the hydrophobicity provided by the attached alkyl chains. In that way, a greater barrier capacity can be observed in coatings containing 20% [*p*-O(C_4H_9)coum] MA and 20% [*p*-O(C_6H_{13})coum] MA inhibitors. The Bode plots (Fig. 3B) show the impedance response of coatings having 20 wt% of [*p*-OHcoum] MA, [*p*-O(C_4H_9)coum] MA and [*p*-O(C_6H_{13})coum] MA during an immersion on 0.005 M NaCl aqueous solution for 24 h. The control coating (Fig. S9B, ESI†) shows a decrease in the impedance and in the plateau of the phase angle in the low frequency range with time. The initiation of corrosion can be the main factor for this variation (Fig. S9A, ESI†). Mild steel coated with [*p*-OHcoum] MA based polymer shows an almost constant impedance value ($10^{3,8}$ Ω) and phase angle (27°) throughout the 24 hours at the low frequency range. The coating containing 20% [*p*-O(C_4H_9)coum] MA monomer, presents an initial impedance value of $10^{4.4}$ Ω at the low frequency range. For the corresponding phase angle a peak of 40° is observed. The impedance then reduces over 24 hours to $10^{3.4}$ Ω while the phase angle peak reduces to around 32°. [*p*-O(C_6H_{13})coum] MA based coating shows an impedance of $10^{4.4}$ Ω at the low frequency range after 2 h of immersion in NaCl 0.005 M aqueous solution. This impedance is reduced to $10^{4.2}$ Ω after 9 h and it remains constant until 24 h. In the corresponding phase angle of the time constant (Fig. 3B(f)) various peaks can be seen, in contrast to what was observed when the monomer was added to the solution (as discussed above). The multiple phase angles represent different processes and are not simply related to the coating barrier properties or inhibition. Previous work with sol–gel coatings has also reported multiple time constants and these relate to water absorption in the coating as well as porosity in addition to the inhibition processes.[22,25–27] Furthermore, all the coatings present a depressed semicircle in the Nyquist plot (Fig. S8, ESI†) where the sample coated with [*p*-O(C_6H_{13})coum] MA based polymer has the biggest arc consistent with the largest impedance observed in the Bode plot. As with the complex phase angle behaviour, the depressed Nyquist plots are indicative of multiple processes and a detailed analysis of these processes is beyond the scope of this paper. However, combining the impedance values with the observations of the coated specimens post immersion, it is very evident that the coatings with 20% [*p*-O(C_6H_{13})coum] MA provides significantly more protection than any of the other coatings, consistent with the behaviour of the monomer in solution.

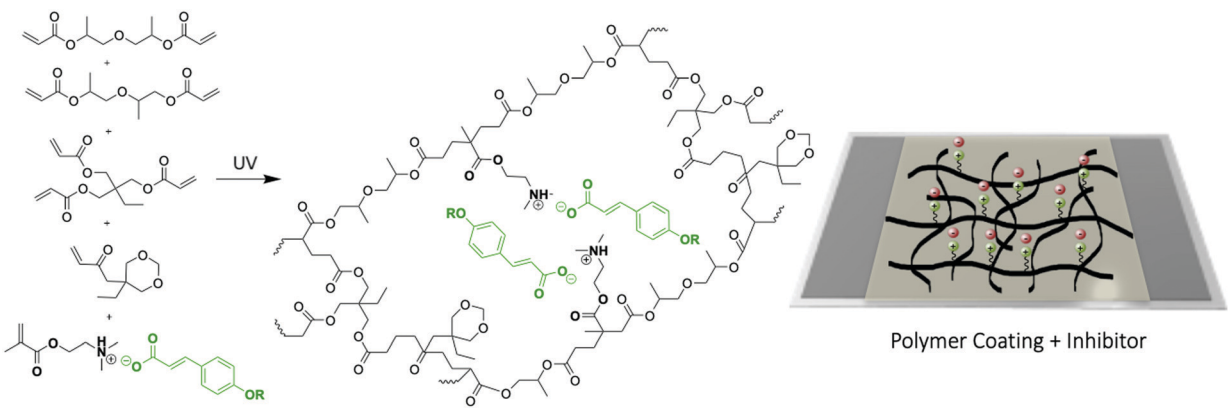

Scheme 1 Chemical structures of monomers and polymer coatings and the UV-photopolymerization on mild steel 1020 surface.

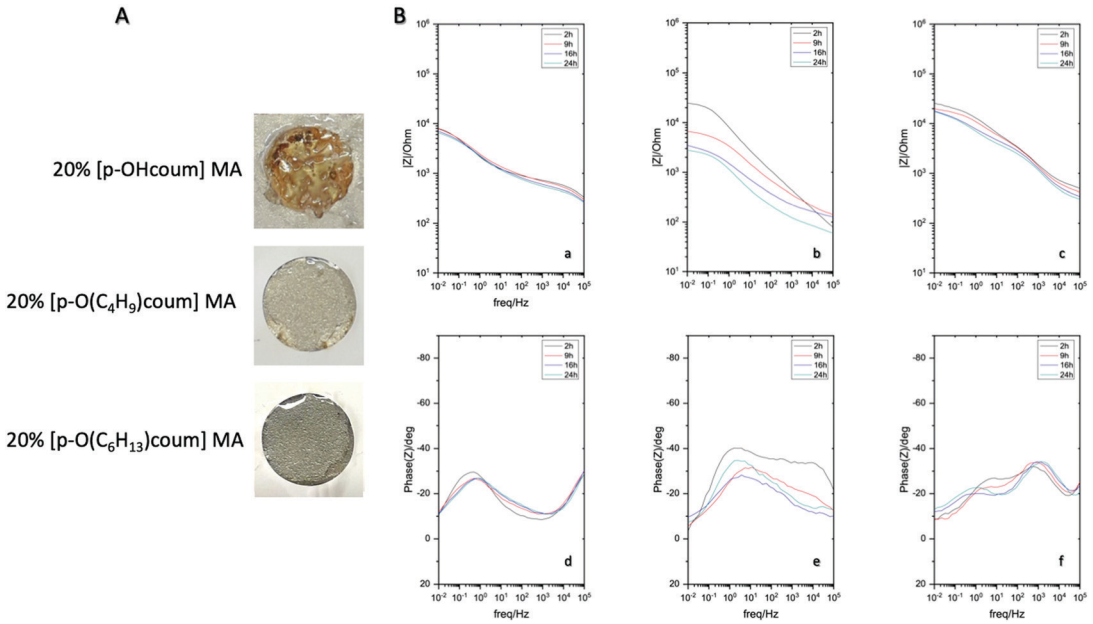

Fig. 3 Polymer coatings on AS1020 mild steel containing 20% of [*p*-OHcoum] MA, 20% of [*p*-O(C_4H_9)coum] MA, and 20% of [*p*-O(C_6H_{13})coum] MA immersed in 0.005 M NaCl after 20 h (A) and electrochemical impedance spectra for different polymer coatings on AS1020 mild steel immersed in 0.005 M NaCl: impedance modulus and phase angle plots for inhibited coating containing 20% [*p*-OHcoum] MA (a and d); inhibited coating containing 20% [*p*-O(C_4H_9)coum] MA (b and e); inhibited coating containing 20% [*p*-O(C_6H_{13})coum] MA (c and f) (B).

Conclusions

In this communication, we report new coumarate containing polymerizable ionic compounds which show great potential as corrosion inhibitors. Potentiodynamic polarisation, electrochemical impedance spectroscopy experiments and surface analyses were made in order to verify the corrosion inhibition performance of the monomers and coatings on the mild steel AS1020 surface. Experiments show that the coumarate ionic monomers reduced mainly the anodic corrosion reaction. Among them, the [*p*-O(C_6H_{13})coum] MA monomer which is the most hydrophobic one presents the best inhibitor profile with the highest inhibition efficiency of 99.6% in solution. The monomers were easily incorporated into polymer coatings by UV-photopolymerizations. The incorporation of the ionic monomers into the commercial polymer coatings formulation significantly improved their corrosion inhibition properties suggesting this is a promising route forward to improve corrosion protective coatings for metal substrates. Further work is being carried out to explain the anticorrosion mechanism of the coumarate based organic ionic compounds.

Conflicts of interest

There are no conflicts to declare.

Acknowledgements

The authors thank for technical and human support provided by IZO-SGI SGIker of UPV/EHU. The authors would like to thank the European Commission for financial support through funding from the European Union's Horizon 2020 Research and Innovation Program under the Marie Sklodowska-Curie grant agreement no. 823989. E. U. thanks the Spanish MINECO for a FPU fellowship. A. E. S. and M. F. are grateful for funding from the Australian Research Council through a Discovery Project, DP180101465.

Notes and references

1 G. Gomes, M. Ueda, A. Beloto, R. Nakazat and H. Reuther, *Mater. Res.*, 2005, **8**, 387–389.
2 Y. Peng, A. Hughes, G. Deacon, P. Junk, B. Hinton and M. Forsyth, *Corros. Sci.*, 2018, **145**, 199–211.
3 A. Chong, J. Mardel, D. MacFarlane, M. Forsyth and A. Somers, *ACS Sustainable Chem. Eng.*, 2016, **4**, 1746–1755.
4 E. Mattsson, *IOM Communications*, 2001.
5 J. Sinko, *Prog. Org. Coat.*, 2001, **42**, 267–282.
6 M. Forsyth, M. Seter, B. Hinton, G. Deacon and P. Junk, *Aust. J. Chem.*, 2011, **64**, 812.
7 M. Forsyth, C. Forsyth, K. Wilson, T. Behrsing and G. Deacon, *Corros. Sci.*, 2002, **44**, 2651–2656.
8 M. Seter, B. Hinton and M. Forsyth, *J. Electrochem. Soc.*, 2012, **159**, C181–C189.
9 F. Blin, S. Leary, G. Deacon, P. Junk and M. Forsyth, *Corros. Sci.*, 2006, **48**, 404–419.
10 M. Forsyth, C. M. Forsyth, K. Wilson, T. Behrsing and G. Deacon, *Corros. Sci.*, 2002, **44**, 2651–2656.
11 O. Riggs, *NACE Int.*, 1973, 7–27.
12 A. Mercer, *Proceedings of the 5th European Symposium on Corrosion Inhibitors Conference*, 1980.
13 G. Wilcox, D. Gabe and M. Warwick, *Corros. Rev.*, 1986, **6**, 327.

14 G. Deacon, P. Junk, W. Lee, M. Forsyth and J. Wang, *New J. Chem.*, 2015, **39**, 7688–7695.
15 M. Frey, S. Harris, J. Holmes, D. Nation, S. Parsons and P. Tasker, *et al.*, *Angew. Chem., Int. Ed.*, 1998, **37**(23), 3245–3248.
16 M. Frey, S. Harris, J. Holmes, D. Nation, S. Parsons, P. Tasker and R. Winpenny, *Chem. – Eur. J.*, 2000, **6**, 1407–1415.
17 B. Brycki, I. Kowalczyk, A. Szulc, O. Kaczerewska and M. Pakiet, *Intechopen*, 2018, **1**, 3–33.
18 A. Chong, M. Forsyth and D. MacFarlane, *Electrochim. Acta*, 2015, **159**, 219–226.
19 S. Tawfik, *J. Mol. Liq.*, 2016, **216**, 624–635.
20 K. Jüttner, *Electrochim. Acta*, 1990, **35**, 1501–1508.
21 O. Al-Rashed and A. Nazeer, *J. Mol. Liq.*, 2019, **288**, 111015.
22 M. Fedel, E. Callone, S. Diré, F. Deflorian, M. G. Olivier and M. Poelman, *Electrochim. Acta*, 2014, **124**, 90–99.
23 A. Yousefi, S. Javadian, N. Dalir, J. Kakemam and J. Akbari, *RSC Adv.*, 2015, **5**, 11697–11713.
24 M. Seter, G. M. A. Girard, W. W. Lee, G. Deacon, P. Junk, B. Hinton and M. Forsyth, *AIMS Mater. Sci.*, 2015, **2**, 1–15.
25 M. Fedel, M. Poelman, M. Zago, C. Vandermiers, D. Cossement, M. G. Olivier and F. Deflorian, *Surf. Coat. Technol.*, 2014, **274**, 9–17.
26 C. Agustín, E. Martín, J. B. Jorcin, G. Imbuluzqueta, P. S. Coloma and U. Izagirre, *J. Sol-Gel Sci. Technol.*, 2019, **89**, 264–284.
27 B. Chico, J. C. Galvàn, D. de la Fuente and M. Morcillo, *Prog. Org. Coat.*, 2007, **60**, 45–53.